World Scientific
www.worldscientific.com

JAPAN SOCIETY OF CIVIL ENGINEERS
COASTAL ENGINEERING COMMITTEE

Coastal Engineering Journal, Vol. 45, No. 2 (2003) 235–253

BRAGG SCATTERING OF WATER WAVES BY MULTIPLY COMPOSITE ARTIFICIAL BARS

TAI-WEN HSU*
Department of Hydraulic and Ocean Engineering, National Cheng Kung University, Da-Shue Rd. 1, Tainan 701, Taiwan
twhsu@mail.ncku.edu.tw

LI-HUNG TSAI
Center of Harbor and Marine Technology, Institute of Transportation, Ministry of Transportation and Communications, W uchi, Taichung 435, Taiwan
ali@mail.ihmt.gov.tw

YING-TSUN HUANG
Department of Hydraulic and Ocean Engineering, National Cheng Kung University, Da-Shue Rd. 1, Tainan 701, Taiwan
hyt527@mail.ncku.edu.tw

Received 5 August 2002
Revised 25 February 2003

A numerical model is developed to investigate the Bragg scattering of water waves by multiply composite artificial bars. Zhang *et al.*'s hyperbolic equation (1999) is recast into an Evolution Equation for the Mild-Slope Equation (EEMSE). It has the advantage to economize computing time for practical application to a large coastal area. The characteristics of both normal and oblique incident waves on the Bragg scattering are investigated. Numerical computations are compared fairly with laboratory experiments. Numerical examples indicate that the performance of the Bragg resonance for multiply composite artificial bars can be greatly improved by increasing both the relative bar height and the number of bars with different intervals. The resulting higher-order harmonic components of the Bragg resonance are shown to be significant, and increase the bandwidth of high performance. The present results can provide an appropriate selection of a multiply composite artificial bar field to a practical design.

Keywords: Bragg resonance; mild-slope equation; composite artificial bars.

*Corresponding author.

1. Introduction

In the past decade, many researchers have studied surface wave scattering caused by the patches of bottom undulations. These studies contain theoretical, experimental, and numerical researches. Their results indicate that the mechanism of a resonant Bragg reflection occurs when the wavelength of the bottom undulation is one half the wavelength of the surface wave (Davies and Heathershaw, 1984; Mei, 1985). Further studies on the comparison between the numerical computations and the laboratory experiments have been made by Dalrymple and Kirby (1986), Kirby (1986), Benjamin *et al.* (1987), and Hara and Mei (1987).

For a single sinusoidal bed, it is noted that not only the primary resonance at $2k/K = 1$ but also the second-harmonic at $2k/K = 2$ can be found (Davies *et al.*, 1989; O'Hare and Davies, 1993), where $k = 2\pi/L$ and $K = 2\pi/\ell$ are free-surface wavenumber and bottom wavenumber, respectively, and L and ℓ are free-surface wavelength and bottom wavelength. In the case of the bottom consisting of the superposition of two sinusoids having two different wavenumbers, K_1 and K_2 ($K_2 > K_1$), the higher-order harmonic of Bragg resonances were revealed. Resonances corresponding to $k = (K_2 - K_1)/2$, which occur at low frequency, are referred to as sub-harmonic resonance, and those associated with $k = K_1$, $k = K_2$, and $k = (K_2 + K_1)/2$, which occur at large frequency, are referred to as high-harmonic resonances by Belzons *et al.* (1991) and Guazzelli *et al.* (1992). On the other hand, the experiments addressed when the relative bed amplitude b/h is increased, the center of the bands for the Bragg reflection is slightly shifted toward lower values of $2k/K$, where b is the amplitude of the bottom undulation and h is the mean water depth of a horizontal bed. By dividing the bottom into a series of small shelves, a step approximation model (Guazzelli *et al.*, 1992) and a successive application matrix (O'Hare and Davies, 1993) have been used to reproduce this phenomenon. They proved the accuracy and validity of the method with the theoretical solutions calculated by the eigenfunction expansion method (Kirby and Dalrymple, 1983; Liu, 1983). However, the effects of evanescent modes are not included in the model, as their numerical results under predicted the sub-harmonic resonance. More recently, Cho and Lee (2000) applied a theoretical model based on the eigenfunction expansion method to study the Bragg scattering of monochromatic waves over an arbitrary topography. The evanescent modes as well as the propagating modes, are considered in the model. The influence of normal and inclined incidence of surface waves on the Bragg reflection is also examined. In their calculation, the representation of the bottom topography by a large finite number of small steps requires a large amount of computing time. This treatment renders the model inefficient on the application to a large coastal area.

Alternative numerical models representing extensions of the Mild-Slope Equation (MSE), derived by Berkhoff (1972), have also been developed. Chamberlain and Porter (1995) improved the MSE to propose a Modified Mild-Slope

Equation (MMSE), which includes the higher-order bottom effect terms. Suh *et al.* (1997) developed a Hyperbolic Mild-Slope Equation (HMSE) for wave propagation over rapidly varying topography. Lee *et al.* (1998) recast the HMSE into the form of a pair of first-order equations. Their results showed that HMSE has the same accuracy as those using MMSE. Following Li (1994), Hsu and Wen (2001) extended the Lee *et al.*'s (1998) equation to a Parabolic Mild-Slope Equation (PMSE) to account for rapidly varying topography. Kirby (1986) extended the MSE to include small-amplitude deviations from the slowly varying water depth. This Extended Mild-Slope Equation (EMSE) is limited in predicting sub-harmonic resonances caused by steep doubly-sinusoidal bars as reported by O'Hare and Davies (1993). This is because the EMSE neglects the higher-order terms, which are particularly important for steep undulations or rapidly varying topography. Zhang *et al.* (1999) developed a Hybrid Model (HM) by extending the EMSE to the case of monochromatic waves over a steep undulating bottom. The higher-order terms neglected in the EMSE are retained, which enhance the overall prediction capability for steep ripple beds. However, the HM is a hyperbolic equation marching in the time domain, in which the integration over a large number of wave periods with small time step is required. Many computational efforts are created using this procedure. Moreover, the HM is only applied to normally incident waves over the sinusoidal bottom. The effects of the oblique waves are not considered, which therefore limit the model application for practical engineering problems.

The studies mentioned above only concerns the Bragg scattering of surface waves over sinusoidal bars, which are naturally formed off beaches by partially or fully standing waves. A practical design using the patches of sinusoidal configurations is not feasible in a coastal engineering technique. For this problem, Mei *et al.* (1988) proposed the concept of the Bragg breakwaters to protect the drilling platform from wave attack on the oil fields in the Ekofisk of the North Sea. Based on their studies, the potential effectiveness against waves appears to be reasonable. Kirby and Anton (1990) and Bailard *et al.* (1992) also have investigated similar idea. Kirby and Anton presented a theory based on Miles (1981) and EMSE to the study of periodically spaced artificial bars with rectified sine geometry. The solutions of both resonant reflection and nonresonant reflection are obtained through theoretical analysis and numerical calculation. Bailard *et al.*'s (1992) numerical results indicated that a staggered nine-element bar field can provide a 25% reduction in storm erosion volume along the beaches on the US Gulf Coast and the Atlantic Coast. The bandwidths of primary and higher-order harmonic resonances are narrow in their numerical examples, and thus, Bailard *et al.* (1992) concluded that the application of a Bragg breakwater might be limited in practice for most US beaches. According to Zhang *et al.* (1999), this limitation can be improved by using multiply superposed bottom undulations to produce both primary and higher-order harmonic resonances. They showed that both magnitude and bandwidth of the Bragg resonance peaks increase, by increasing the number of sinusoidal components and the amplitude of ripple beds.

As an extension of the PMSE of Hsu and Wen (2001), we present an Evolution Equation of Mild-Slope Equation (EEMSE) based on Zhang *et al.*'s (1999) HM to investigate the Bragg scattering over multiply composite artificial bars with rectangular geometry. The higher-order terms, neglected in PMSE for steep undulations of artificial bars, are retained in the present model. Comparisons of numerical results and laboratory experiments are made to examine the prediction capability of EEMSE. Numerical examples of the Bragg scattering of planary waves by multiply composite artificial bars are performed. Several multiply combined artificial bars are designed in the numerical examples. In each combination, key parameters, such as the number of bars, relative bar height, relative bar spacing and incident wave angle, are varied to investigate the performance of the Bragg resonance. Finally, a concept to enhance the magnitude and bandwidth of the Bragg resonance peaks for artificial bars is proposed.

2. Numerical Model

2.1. *Model equation*

For model formulation, a Cartesin coordinate (x, y, z) with x = onshore direction, y = alongshore direction, and z = upward direction is used. The depth-averaged wave equation for monochromatic, linear waves propagating over the arbitrary varying bottom topography may be formulated following the Green's second-identity method of Smith and Sprinks (1975) or Liu (1983). A bottom function, $h'(x, y)$, consisting of a slowly varying component and a rapidly varying component, is expressed as

$$h'(x, y) = h(x, y) - \delta(x, y) \tag{1}$$

where $\delta(x, y)$ represents a rapidly varying component over a relatively slowly varying component $h(x, y)$. The Laplace equation, subject to linearized free-surface boundary conditions and bottom boundary condition are written, respectively, as

$$\nabla_h^2 \Phi + \Phi_{zz} = 0, \quad \text{at } -h'(x, y) \leq z \leq 0 \tag{2}$$

$$\Phi_{tt} + g\Phi_z = 0, \quad \text{at } z = 0 \tag{3}$$

$$\Phi_z = -\nabla_h h \cdot \nabla_h \Phi + \nabla_h \delta \cdot \nabla_h \Phi, \quad \text{at } z = -h'(x, y) \tag{4}$$

in which $\Phi(x, y, z, t)$ is the velocity potential; $\nabla_h = (\partial/\partial x, \partial/\partial y)$ the horizontal gradient operator; t the time; and g the gravitational acceleration. Following Kirby (1986), the solution of Eq. (2) may be expressed as

$$\Phi(x, y, z, t) = f(x, y, z)\tilde{\phi}(x, y, t) + \sum \text{non-propagating models} + O(k\delta) \tag{5}$$

Using Green's second-identity to neglect non-propagating modes, Eq. (2) is integrated with respect to z from the bottom to the surface:

$$\int_{-h}^{0} f\Phi_{zz}dz - \int_{-h}^{0} \Phi f_{zz}dz = [f\Phi_z - \Phi f_z]_{-h}^{0} \tag{6}$$

where

$$f = \frac{\cosh k(z+h)}{\cosh kh} \tag{7}$$

is a slowly varying function in the x, y plane. The integrals of Eq. (6) are manipulated to obtain the following equation (Zhang *et al.*, 1999):

$$\tilde{\phi}_{tt} - \nabla_h \cdot (CC_g\nabla_h\tilde{\phi}) + (\omega^2 - k^2CC_g)\tilde{\phi} + g(1-\lambda^2)\nabla_h \cdot (\delta\nabla_h\tilde{\phi})$$
$$- g(2\vec{F}_1 \cdot \delta\nabla_h\tilde{\phi} + \vec{F}_1 \cdot \nabla_h\delta\tilde{\phi} + F_2\tilde{\phi}) = 0 \tag{8}$$

where

$$\vec{F}_1 = \lambda(1-\lambda^2)(k\nabla_h h + h\nabla_h k) \tag{9}$$

$$F_2 = \alpha_1(\nabla_h h)^2 k + \alpha_2\nabla_h^2 h + \alpha_3\nabla_h k \cdot \nabla_h h/k + \alpha_4\nabla_h^2 k/k^2 + \alpha_5(\nabla_h k)^2/k^3 \tag{10}$$

C and C_g are the wave celerity and the group velocity, respectively, $\lambda = \tanh kh$. The parameters $\alpha_i (i = 1, 5)$ are

$$\alpha_1 = -\lambda(1-\lambda^2)(1-\lambda q) - 2(1-\lambda^2)\lambda^2 k\delta \tag{11}$$

$$\alpha_2 = -\lambda q(1-\lambda^2)/2 + (1-\lambda^2)\lambda k\delta \tag{12}$$

$$\alpha_3 = q(1-\lambda^2)(2q\lambda^2 - 5\lambda/2 - q/2) - 2(1-\lambda^2)(2\lambda^2 q - \lambda - q)k\delta \tag{13}$$

$$\alpha_4 = q(1-\lambda^2)(1-2\lambda q)/4 - \lambda/4 + (1-\lambda^2)\lambda q k\delta \tag{14}$$

$$\alpha_5 = q(1-\lambda^2)(4\lambda^2 q^2 - 4q^2/3 - 2\lambda q - 1)/4 + \lambda/4 + (1-\lambda^2)q^2(1-2\lambda^2)k\delta \tag{15}$$

where the notation $q = kh$ is used for convenience. The detailed derivation can be found in the paper of Zhang *et al.* (1999). The rapidly-varying terms, $\nabla_h h$ and $\nabla_h^2 h$, neglected in the EMSE (Kirby, 1986), are retained to increase the prediction capability for steep bottom undulations. In Eq. (8), Kirby's (1986) equation can be recovered if $\vec{F}_1 = F_2 = 0$, and Chamberlain and Porter's (1995) equation can be attained if $\delta = 0$.

To the leading order, the linear dispersion equation can be obtained from Eqs. (3) and (5):

$$\omega^2 = gk\tanh kh \tag{16}$$

where ω is the angular frequency. Writing the velocity potential as $\tilde{\phi} = Ae^{is}$ and using the relationship $\vec{k} = \nabla_h S$, $\tilde{\omega} = -\partial S/\partial t$, Eq. (8) can be split into the real and the imaginary parts, where A is the wave amplitude, $S = \int \vec{k} \cdot d\vec{x} - \tilde{\omega}t$ the phase function, $\vec{k} = k\cos\theta \mathbf{i} + k\sin\theta \mathbf{j}$ the wavenumber vector, θ the wave angle, $\vec{x} = x\vec{i} + y\vec{j}$ the position vector, $\tilde{\omega}$ the total angular frequency, and $i = \sqrt{-1}$ the unit complex variable. It has been shown by Zhang *et al.* (1999) that the real part represents the total dispersion relation combining with the linear dispersion relation and the dispersion relation due to bottom undulation. The total dispersion relation is given by

$$\tilde{\omega}^2 = \omega^2 - CC_g k^2 + \frac{A_{tt}}{A} - gF_2 - gF_3\frac{\nabla_h^2 A}{A} - g\vec{F}_4 \cdot \frac{\nabla_h A}{A} + gF_3 k^2 \tag{17}$$

where

$$F_3 = \frac{CC_g}{g} - (1-\lambda^2)\delta \tag{18}$$

$$\vec{F}_4 = \frac{\nabla_h(CC_g)}{g} - (1-\lambda^2)\nabla_h\delta + 2\delta\vec{F}_1 \tag{19}$$

From Eq. (17), it is noted that the total dispersion relation departs from the linear dispersion relation, while the phase function changes from $S = \int \vec{k} \cdot d\vec{x} - \omega t$, to a new phase function, $\tilde{S} = \int \vec{k} \cdot d\vec{x} - \tilde{\omega}t$. The wave celerity C and group velocity C_g thus depend on bottom variations. Due to this dispersion behavior, the peak of the Bragg resonance will shift slightly toward the lower values of $2k/K$, as observed in the laboratory. Equations (8) and (17) also indicate that the higher-order harmonic resonances are affected by higher-order terms including the bed undulation $\nabla_h\delta$, the bottom slope $\nabla_h h$, and curvature $\nabla_h^2 h$.

2.2. *EEMSE model*

The HM is based on a time-dependent hyperbolic equation, which consumes a large amount of computing time to achieve the convergence of the program for a large coastal area (Hsu and Wen, 2001). Furthermore, the model is usually unable to perform calculations for the case of wide-angle wave incidence (Maa *et al.*, 2000). In this paper, we developed an EEMSE model on the basis of PMSE proposed by Hsu and Wen (2001) to study the interaction between surface waves and artificial bars with steep variations.

Following the procedure outlined by Hsu and Wen (2001), we introduce a slow coordinate for the time variable, $\bar{t} = \varepsilon t$, and assume $\tilde{\phi}(x, y, t, \bar{t}) = \phi(x, y, \bar{t})e^{-i\omega t}/\sqrt{[CC_g - g(1-\lambda^2)\delta]}$ (ε = a perturbation parameter of order $O(\nabla_h h/kh)$) to obtain an evolution equation for the mild-slope equation from

Eq. (8):

$$\left[\frac{-2\omega i}{CC_g - g(1-\lambda^2)\delta}\right]\left(\frac{\partial\phi}{\partial t}\right)$$

$$= \nabla_h^2\phi + k_c^2\phi + \frac{g}{\sqrt{CC_g - g(1-\lambda^2)\delta}}\left[2\vec{F}_1\cdot\delta\nabla_h\frac{\phi}{\sqrt{CC_g - g(1-\lambda^2)\delta}}\right]$$

$$+ \frac{\delta}{\sqrt{CC_g - g(1-\lambda^2)\delta}}\nabla_h[g(1-\lambda^2)]\cdot\nabla_h\left[\frac{\phi}{\sqrt{CC_g - g(1-\lambda^2)\delta}}\right] \quad (20)$$

where

$$k_c^2 = \left[\frac{g\vec{F}_1\cdot\nabla_h\delta + gF_2 + k^2CC_g}{CC_g - g(1-\lambda^2)\delta}\right] - \frac{\nabla_h^2\sqrt{CC_g - g(1-\lambda^2)\delta}}{\sqrt{CC_g - g(1-\lambda^2)\delta}} \quad (21)$$

is a pseudo wave number. As reported by Hsu and Wen (2001), the EEMSE has the benefit of saving the storage and computing time for a large computational domain when compared with the hyperbolic equation of HM.

2.3. *Boundary conditions and numerical procedure*

The radiation boundary conditions are specified to ensure that waves must go out radially from a computed area with decreasing amplitude. There are two types of boundary conditions — a partial reflection boundary condition, and a given boundary condition. These boundary conditions reduce the reflected waves from the boarder to the computational domain. According to Hsu and Wen (2001), the boundary conditions are given as follows.

$$\frac{\partial\phi}{\partial x} = \pm(-1)^m i\alpha k\cos\theta\phi + 2ik\cos\theta\phi_i, \quad \text{on } \pm x \quad (22a)$$

$$\frac{\partial\phi}{\partial y} = \pm(-1)^m i\alpha k\sin\theta\phi + 2ik\sin\theta\phi_i, \quad \text{on } \pm y \quad (22b)$$

where $\alpha = (1-R)/(1-R)$ is an absorption coefficient, R, the reflection coefficient, and the subscript, "i", denotes a quantity of the incident wave. For the partial reflection boundary, $\phi_i = 0$, $m = 0$, and $0 < \alpha \leq 1$. For the given boundary condition, $m = 1$, $\alpha = 1$, and $\phi_i = (Ag/\omega)e^{iS_0}$ is given, where $S_0 = kx\cos\theta_i + ky\sin\theta_i - \omega t$, θ_i, the incident wave angle. The finite difference method and Alternating Direction Implicit (ADI) scheme are employed for the solution of Eq. (20), subject to the boundary conditions of Eq. (22). For details of the numerical scheme, see Hsu and Wen (2001).

For inclined wave incidence, the approaching wave angles are unknown. For a given initial guess θ_i, the wave number $\vec{k}$ can be found from $\vec{k} = \nabla_h S$, and the phase function S can be solved from $S = \tan^{-1}[\mathrm{Im}(\phi)/\mathrm{Re}(\phi)]$ (Re and Im are the real and

imaginary part of a complex variable, respectively). Finally, the approaching wave angle is obtained by an iterative procedure from the equation (Hsu and Wen, 2000):

$$\theta = \tan^{-1} \frac{\partial S/\partial y}{\partial S/\partial y} \tag{23}$$

Hsu and Wen's (2000) numerical examples showed that this method provided a reasonable improvement on the radiation boundary conditions for large wave angle incidence. During the calculation, the iterative procedure is repeated until a residual value is smaller than a tolerance value E. According to Hsu and Wen (2000, 2001), the value of E is smaller than 10^{-4} when the convergence is achieved.

3. Experiments and Model Verification

3.1. *Experimental setup*

To examine the performance of EEMSE, experiments of the Bragg reflections over multiply composite artificial bars are conducted in the hydraulic laboratory at the Center of Harbor and Marine Technology, Taiwan. The wave flume has a dimension of 100 m in length, 1.5 m in width and 2.0 m in height. It is equipped with a piston-type wave generator to make the sinusoidal waves in one end-side, while the other end-side is placed with the absorbing material to dissipate the reflected wave energy. Artificial bars with rectangular geometry are placed discretely on a flat bottom, in the middle region of the wave flume. These undulating beds are varied only in the x-direction along the wave flume, thus the motion of waves are horizontally one-dimensional. The schematic diagram of the wave flume system and experimental setup is given in Fig. 1. In total, eight wave gauges of capacity-type are placed for water surface elevation measurements in this study. One wave gauge in region A is used to measure and to calibrate the incident wave conditions, six wave gauges are installed at region B to estimate the reflected waves using the least squares method developed by Mansard and Funke (1980), and the other one wave gauge is placed at region C to estimate the transmitted waves. The reflected waves by the end-side of the wave flume are negligible because of the long traveling distance and energy

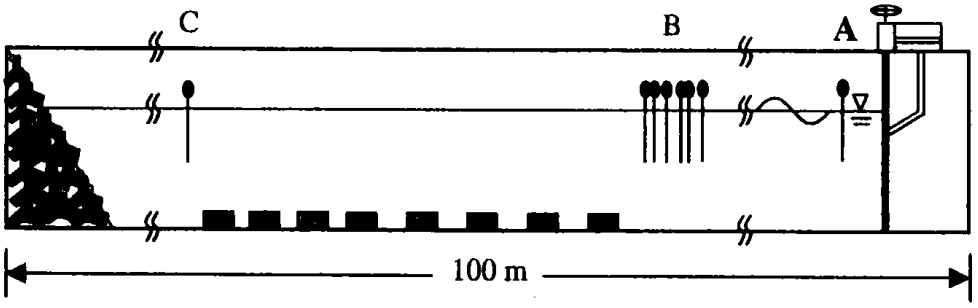

Fig. 1. Wave flume system and experimental setup.

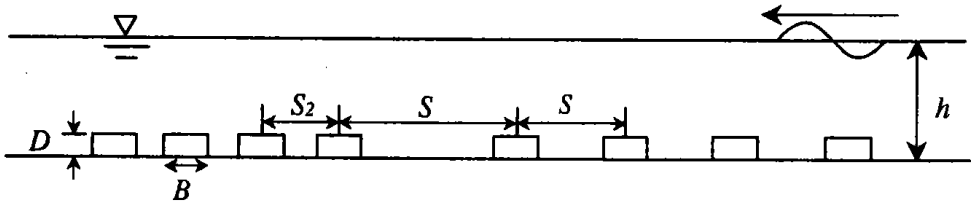

Fig. 2. Schematic diagram and definition of all parameters in a multiply composite artificial bar.

dissipation by the end-side of the flume. Data sampling frequency is 30 Hz to acquire an accurate resolution in the range of the designed wave period.

The incident wave height and period are designed respectively as $H_i = 4$ cm and 1.03 s $\leq T \leq$ 4.03 s to maintain a close assumption of linear wave theory ($0.013 \leq kA \leq 0.077$, $0.006 \leq \hat{S} \leq 0.212$, where $\hat{S} = A/(k^2h^3)$ is the Stokes parameter). The bar footprint is adopted as $B = 60$ cm and water depth is taken to be $h = 60$ cm for all experiments. The schematic diagram and definition of all parameters in multiply composite artificial bars are shown in Fig. 2.

In Fig. 2, two different combinations of multiply composite beds are considered with varying key parameters N_i, D_i/h, S_{i+1}/S_i, and B/S_i, where N_i is the number of bars, D_i is the bar height, and S_i is the bar spacing. The subscript "i", denotes the ith combination of the equal-interval bar spacing, and S_i represents the interval of the adjacent different combination in the ith composite bed. In this study, we use the fixed conditions of $S = S_2$, $N_1 = N_2$, and $N = N_1 + N_2 = 2N_1 = 2N_2$, where N is the total number of artificial bars. The effects of each key parameter on the Bragg scattering due to the multiply composite artificial bars are discussed.

3.2. *Model verification*

Five cases are performed in the experiments. For the composite artificial bars, the bar spacing of $S_1 = 240$ cm and $S_2 = 180$ cm; 240 cm; 300 cm is employed. Numbers of bars used in the experiments are $N = 4$ ($N_1 = N_2 = 2$) and 8 ($N_1 = N_2 = 4$). The values of the relative bar height adopted in the experiments are $D/h = 0.2$ and 0.4. The designed key parameters in the experiments are presented in Table 1.

The influence of higher-order terms including the bottom undulation $\nabla_h\delta$, bottom slope $|\nabla_h h|$, and curvature $\nabla_h^2 h$ on the Bragg resonance is first examined from theoretical formulation. From Eq. (17), it is noted that the total dispersion relation

Table 1. Key parameters of the experiments.

Case	N_1	N_2	N	S_1 (cm)	S_2 (cm)	D (cm)	B (cm)	h (cm)
1	4	4	8	240	180	24	60	60
2	4	4	8	240	180	12	60	60
3	2	2	4	240	180	24	60	60
4	4	4	8	240	240	24	60	60
5	4	4	8	240	300	24	60	60

departs from the linear dispersion relation due to the interaction between the surface wave and undulating bottom. This total dispersion relation indicates that the higher-order Bragg scattering depends on the rapidly-varying oscillation component $\delta(x, y)$. For a large value of bottom undulation, a more accurate approximate solution can be obtained by expanding the steep component with respect to the slowly-varying basic component. In this sense, the present model is different from the PMSE proposed by Hsu and Wen (2001) in which the rapidly-varying component has been neglected.

The numerical results of PMSE ($\delta(x, y) = 0$) and EEMSE ($\delta(x, y) \neq 0$) are presented in Figs. 3–7 with the experimental data for the cases 1–5. We can see that the numerical results of the present EEMSE are in good agreement with the experimental data, while the PMSE results overestimate the primary peaks and bandwidths of the Bragg resonances. The larger the relative bar height is (Figs. 3, 5, 6, and 7), the more the PMSE appears to overestimate the peak value of the Bragg reflection. This result implies that the PMSE neglecting higher-order terms of the bottom undulation is restrictive for bottom undulation scattering problems.

In order to examine the effects of bottom slope and curvature on the performance of the Bragg scattering, a numerical example is performed with sinusoidal bars over a sloping bed. The designed slope is shown in Fig. 8, with each end connecting to a constant-depth region ($h_1 = 180$ cm, $h_2 = 20$ cm). The sinusoidal bars have the bottom wavelength $\ell = 50$ cm, amplitude of bottom undulation $b = 10$ cm, and

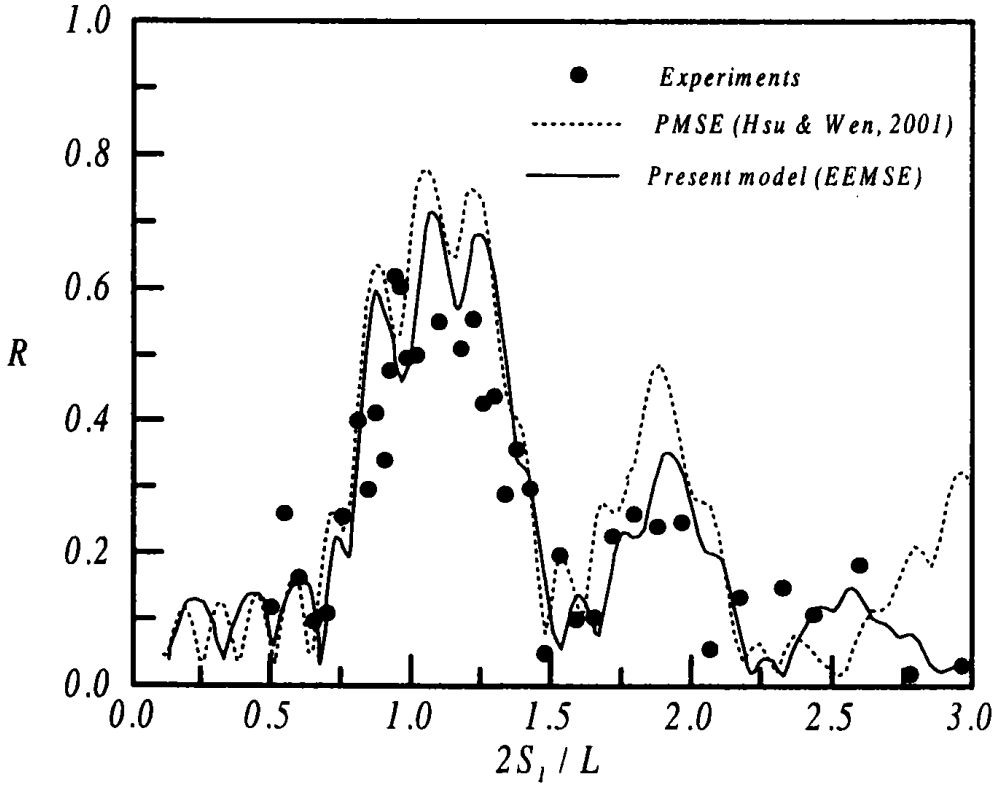

Fig. 3. Results of the reflection coefficient for $N = 8$, $D/h = 0.4$, $S_2/S_1 = 0.75$, and $B/S_1 = 0.25$.

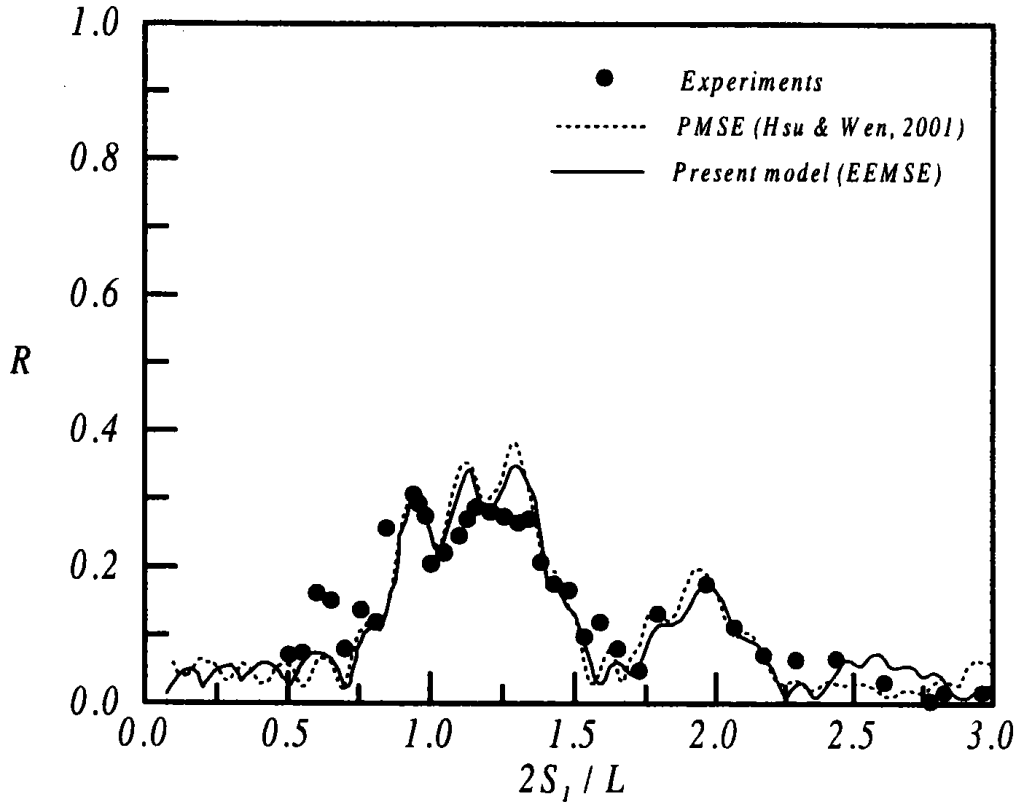

Fig. 4. Results of the reflection coefficient for $N = 8$, $D/h = 0.2$, $S_2/S_1 = 0.75$, and $B/S_1 = 0.25$.

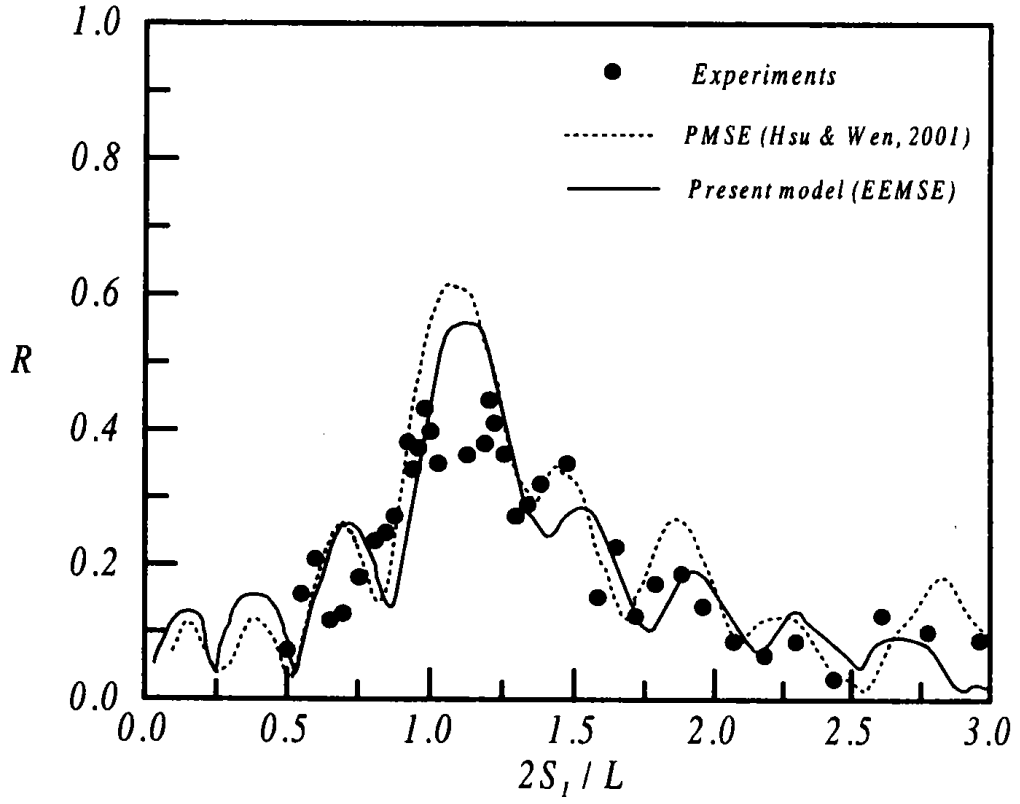

Fig. 5. Results of the reflection coefficient for $N = 4$, $D/h = 0.4$, $S_2/S_1 = 0/75$, and $B/S_1 = 0.25$.

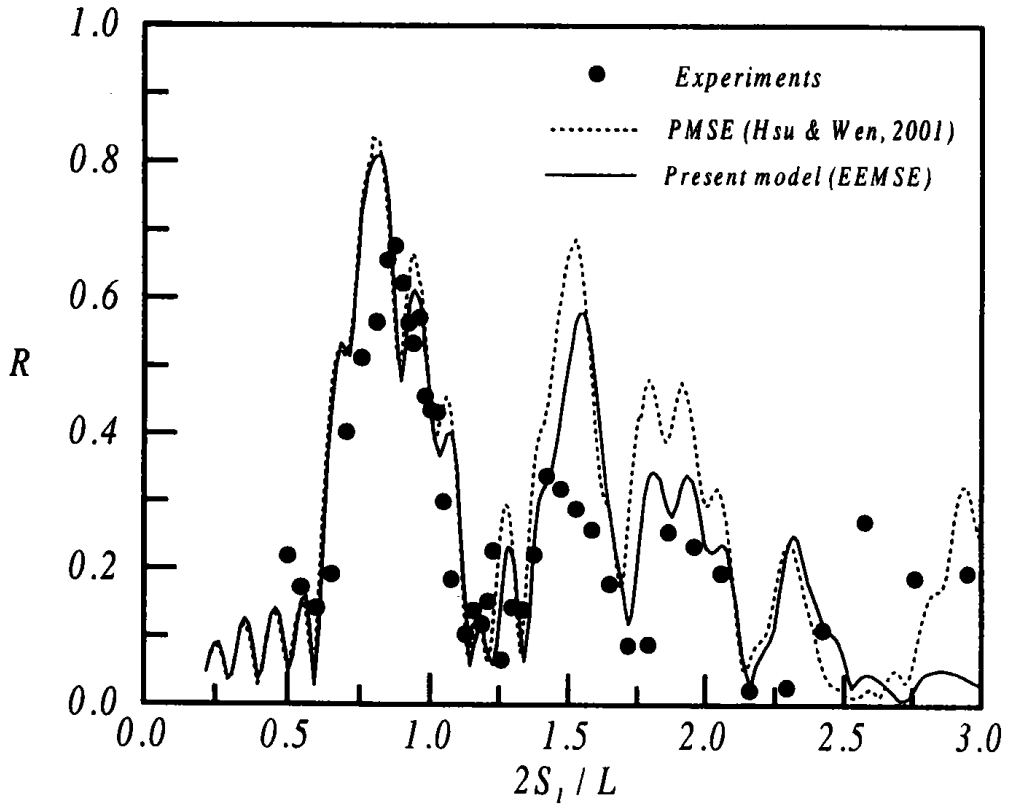

Fig. 6. Results of the reflection coefficient for $N = 8$, $D/h = 0.4$, $S_2/S_1 = 1.25$, and $B/S_1 = 0.25$.

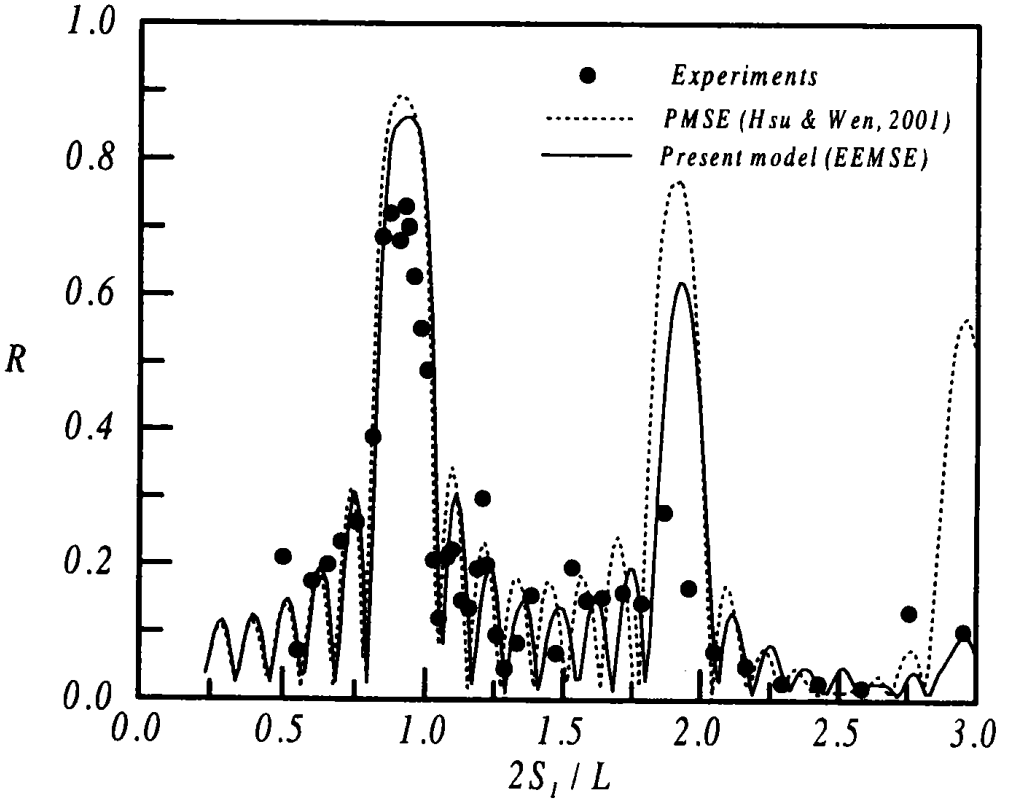

Fig. 7. Results of the reflection coefficient for $N = 8$, $D/h = 0.4$, $S_2/S_1 = 1.00$, and $B/S_1 = 0.25$.

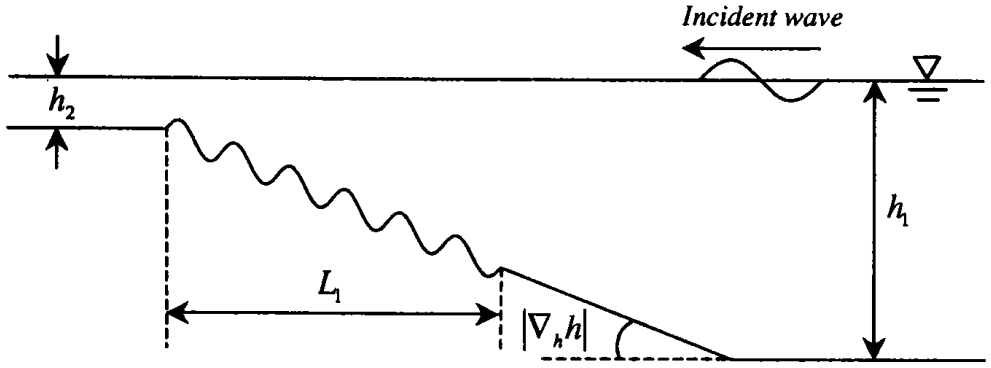

Fig. 8. Sinusoidal bars on a sloping beach.

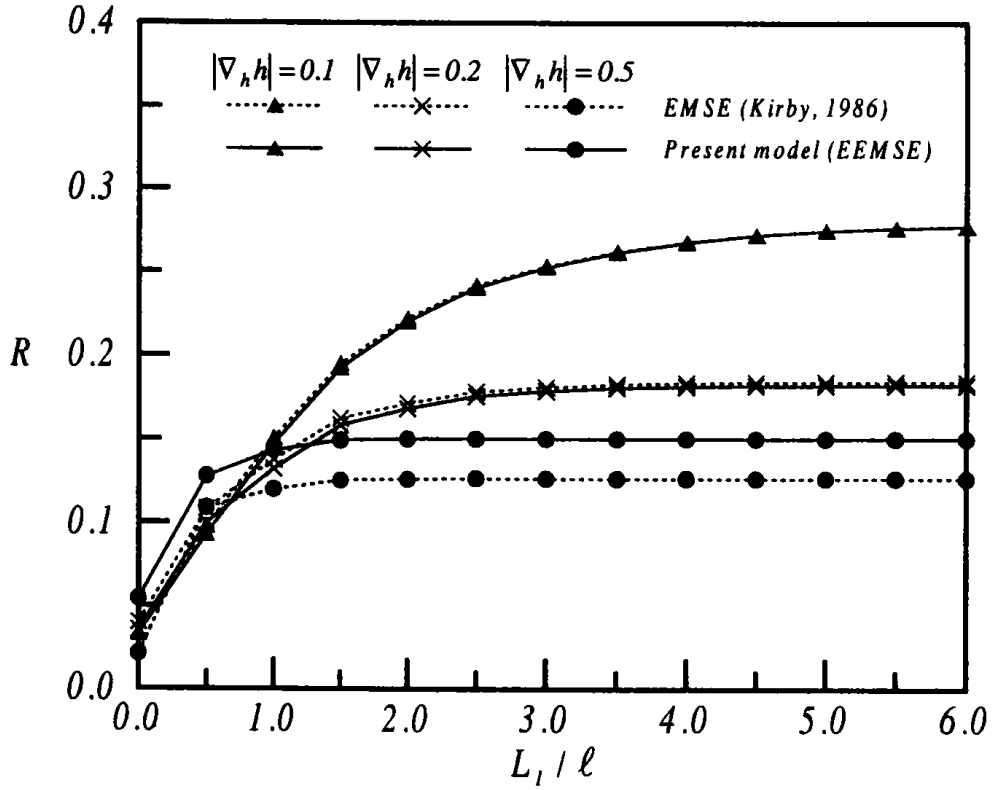

Fig. 9. Comparison of reflection due to sinusoidal bars over sloping beach calculated using various wave models.

total length $0 \leq L_1 \leq 300$ cm. The incident wave is chosen to have a wavelength just twice that of the bottom wavelength, i.e. $2k/K = 1$. The slope is varied to calculate the Bragg reflection coefficient and then compare the results with EMSE proposed by Kirby (1986) in which the bottom slope and curvature are neglected, i.e. $|\nabla_h h| = \nabla_h^2 h = 0$. Figure 9 compares the present model EEMSE and EMSE results with respect to three different slopes ($|\nabla_h h| = 0.1$, 0.2, and 0.5). The result demonstrates that the EMSE results deviate EEMSE as the bottom slope increases. The importance of bottom slope on the Bragg scattering is identified for this numerical example.

4. Results and Discussion

4.1. *The number of bars*

Guazzelli *et al.*'s (1992) experimental results pointed out that the peak amplitude of the Bragg reflection increased and bandwidth decreased for increasing undulated number of the sinusoidal bed. The results of the multiply sinusoidal bed by numerical simulations (Zhang *et al.*, 1999) also showed that the number of the sinusoidal bars would affect the production of higher-order harmonic resonances. A larger number of the sinusoids may result in more possible higher-order harmonic resonances. Therefore, it is possible to enhance the higher-order harmonic resonances by adding the number of artificial bars. The composite beds consisting of three different combinations of artificial bars $N = 4$ ($N_1 = N_2 = 2$), $N = 6$ ($N_1 = N_2 = 3$), and $N = 8$ ($N_1 = N_2 = 4$) under the same conditions of $D/h = 0.4$, $S_2/S_1 = 0.75$, and $B/S_1 = 0.25$ are investigated. In Fig. 10, the results indicate that larger primary and higher-order harmonic Bragg resonances can be found as the number of bars increases. The bandwidth of the primary harmonic resonances at the high performance region also increases while increasing the number of bars. This phenomenon is quite different from the results of the theoretical model obtained by Belzons *et al.* (1991) and Guazzelli *et al.* (1992) on doubly-sinusoidally beds. This is because the positions of two primary resonances caused by two combinations of equal-interval bars

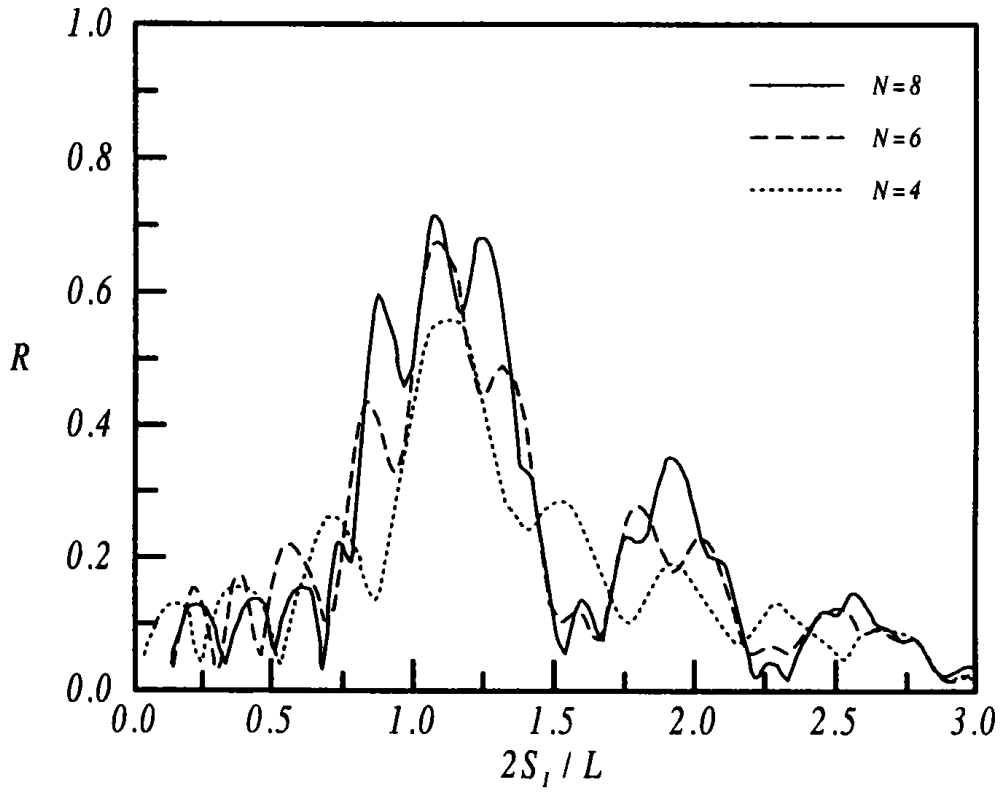

Fig. 10. Reflection coefficients over multiply composite artificial bars with different number of bars ($D/h = 0.4$, $S_2/S_1 = 0.75$, and $B/S_1 = 0.25$).

are very close to producing a larger bandwidth of the primary harmonic resonance at the high performance region.

4.2. *The relative bar height*

Both theories (Guazzelli *et al.*, 1992; Zhang *et al.*, 1999) and experiments (Gazzelli *et al.*, 1992) revealed that a larger bed amplitude, or larger slope for sinusoidal bottom undulations, could increase the peak amplitude and bandwidth of the Bragg reflection. Furthermore, the peaks are shifted toward lower frequencies and yield the higher-order harmonics of the Bragg resonance. To examine the effects on the relative bar heights of multiply composite artificial bars, three kinds of relative bar heights $D/h = 0.2$, $D/h = 0.3$, and $D/h = 4$ under the same conditions $N = 8$ ($N_1 = N_2 = 4$), $S_2/S_1 = 0.75$, and $B/S_1 = 0.25$ are considered in the numerical calculation. Figure 11 shows that both peaks and bandwidths of the primary and higher-order harmonic resonances increase, while increasing the relative bar height. The peaks of the Bragg resonance are slightly shifted toward a lower value of $2S_1/L$ as the relative bar height increases. This shift results from the total dispersion behavior by the interaction between the surface wave and undulating bottom. The phenomenon can also be observed in Guazzelli *et al.*'s (1992) experiments. Comparing with Figs. 10 and 11, it is noted that the reflection caused by the relative bar height increases more significantly than the case caused by the number of bars. This is due to the fact that the relative bar height could enhance the overall wave-blocking efficiency.

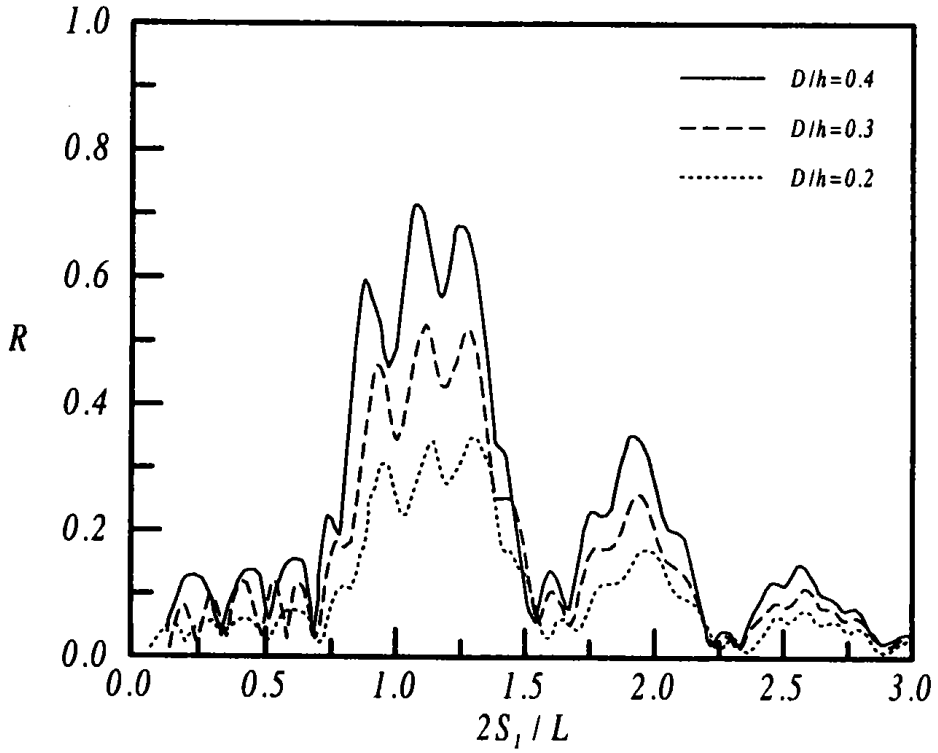

Fig. 11. Reflection coefficients over multiply composite artificial bars with different relative bar heights ($N = 8$, $S_2/S_1 = 0.75$, and $B/S_1 = 0.25$).

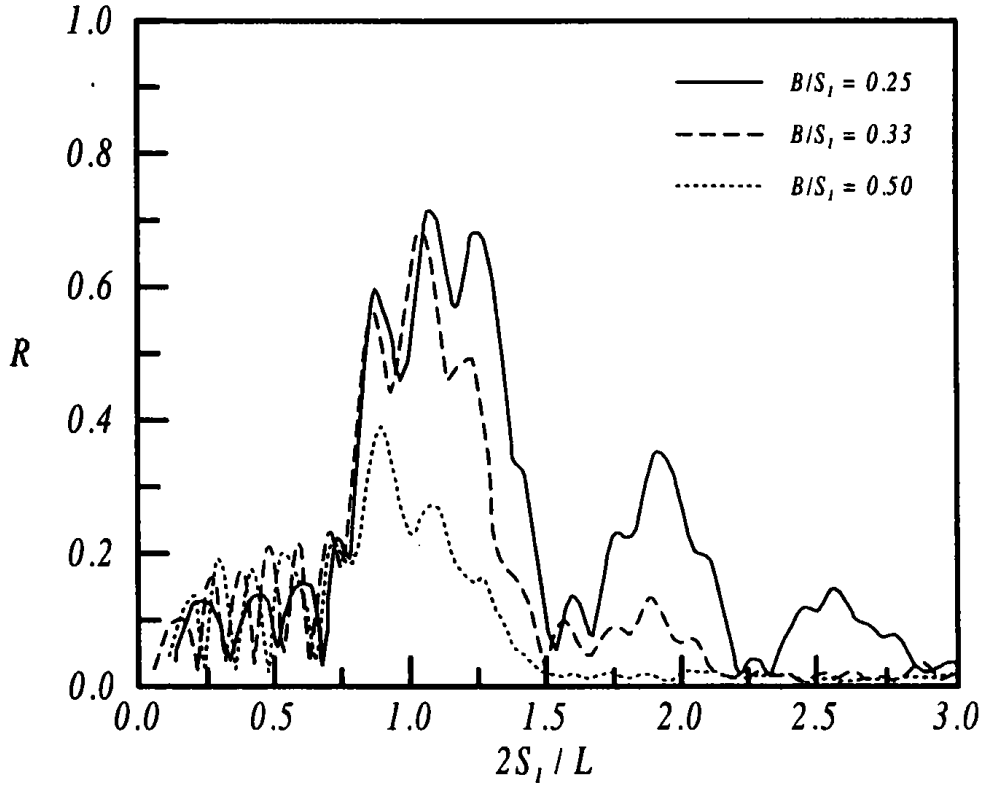

Fig. 12. Reflection coefficients over multiply composite artificial bars with different relative bar spacings ($N = 8$, $D/h = 0.4$, and $S_2/S_1 = 0.75$).

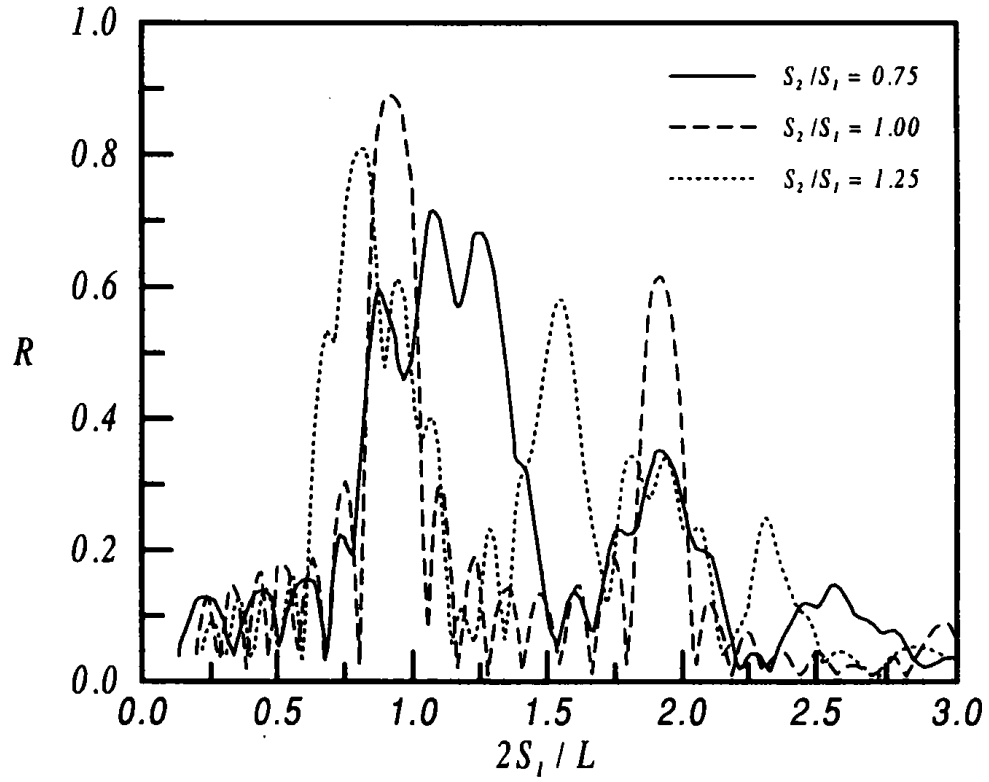

Fig. 13. Reflection coefficients over multiply artificial bars with different ratio of bar spacings ($N = 8$, $D/h = 0.4$, and $B/S_1 = 0.25$).

4.3. *The bar spacing*

Kirby and Anton (1990) showed that the peak value of higher-order harmonic resonance in the reflection coefficient can be adjusted by changing the bar spacing. The importance of higher-order harmonic resonances decreases with a closer bar spacing. Three computed cases of $B/S_1 = 0.25$, $B/S_1 = 0.33$, and $B/S_1 = 0.5$ under the same conditions of $N = 8$, $D/h = 0.4$, and $S_2/S_1 = 0.75$ are presented in Fig. 12. The result indicates that the decrease of the relative bar spacing B/S_1 could increase the amplitude of both primary and higher-order harmonic resonances. However, it is interesting to note that the higher-order harmonics disappear in the case of $B/S_1 = 0.5$. It is concluded that pushing bars closer together could reduce the importance of the higher-order harmonic resonances for the same footprint of bars.

Figure 13 shows the reflection coefficients by multiply composite artificial bars with different spacing ratios of $S_2/S_1 = 0.75$, 1, and 1.25 under the same condition of $N = 8$, $D/h = 0.4$, and $B/S_1 = 0.25$. The EEMSE results are also compared fairly with experimental data. This result illustrates that the bandwidths of both primary and higher-order harmonic resonances become larger under the multiply composite artificial bars conditions ($S_2/S_1 = 0.75$ and 1.25) when comparing with an equal bar spacing ($S_2/S_1 = 1$). Different bar spacing could produce distributive positions of the Bragg reflection. Accordingly, we can achieve the expectable effect on having the appropriate spacing of multiply composite artificial bars to protect the beach-face from the full impact of the waves.

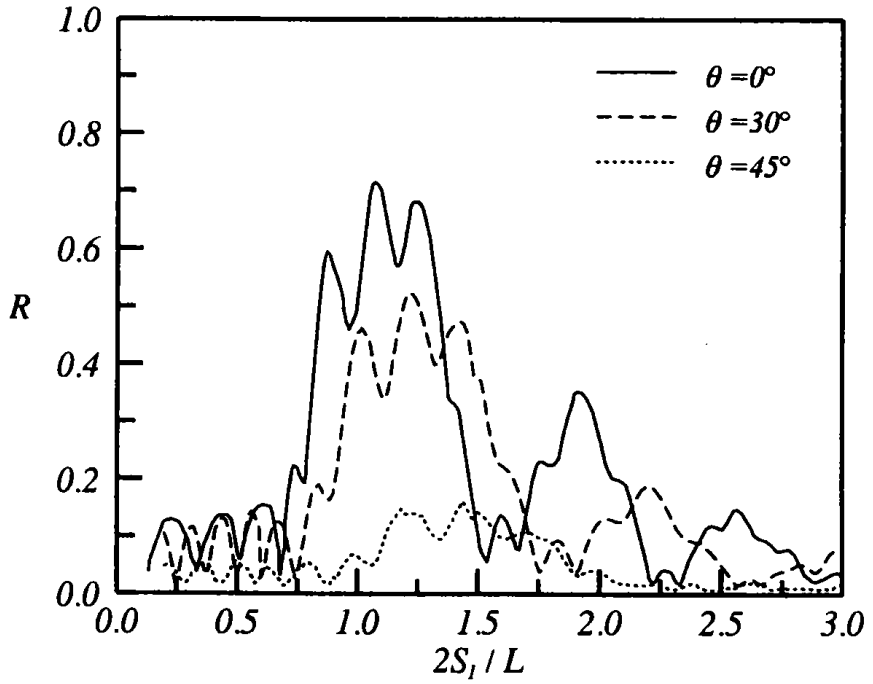

Fig. 14. Reflection coefficients over multiply artificial bars with different incident wave angles ($N = 8$, $D/h = 0.4$, $S_2/S_1 = 0.75$, and $B/S_1 = 0.25$).

4.4. *The incident wave angle*

The model is also used to calculate the reflection coefficients for obliquely incident waves which are not considered in Zhang *et al.*'s (1999) HM. As shown in Fig. 14, the present numerical results depict the reflection coefficients by multiply composite artificial bars with different incident wave angles $\theta = 0°$, $30°$, and $45°$, with the same parameters of Fig. 3. It is noted that the strong shift of the reflection peaks toward higher values of $2S_1/L$ and the magnitude of reflection coefficients becomes smaller while increasing the incident wave angle. This result agrees with predictions by Dalrymple and Kirby (1986) using EMSE and Cho and Lee (2000) using the eigenfunction expansion method.

5. Conclusions

A numerical model based on the Evolution Equation of Mild-Slope Equation (EEMSE) is developed to study the interaction between surface waves and multiply composite artificial bars. As an extension of HM developed by Zhang *et al.* (1999), the present model is applied to the characteristics of the Bragg scattering over multiply composite artificial bars due to the oblique incident wave, which was not considered in the HM. By comparing the experimental measurements with the numerical results of the present model, Kirby's (1986) EMSE (Extended Mild-Slope Equation) and Hsu and Wen's (2001) PMSE (Parabolic Mild-Slope Equation), it shows that the present model is capable of producing accurate results of the primary and higher-order harmonic Bragg resonances over composite artificial bar field.

Using the developed computer programs, the performance of different composite artificial beds under various combinations of the bar number, relative bar height, relative bar spacing, and incident wave angle could be evaluated. When multiply composite artificial bars are used, in addition to the primary peaks, the resulting higher-order harmonic of the Bragg resonances are also found to be significant and greatly increase the bandwidth at the high performance region. Numerical computations show that both the amplitude and bandwidth of each resonant component increase with the increase of the relative bar height, the number of bars, and bar spacing. By putting bars further apart in a composite artificial bed, it could increase the importance of the higher-order harmonic resonant effect. The magnitude of primary Bragg reflection decreases with the increase of incident wave angles. It is concluded that a multiply composite artificial bar field with an appropriate selection of key parameters may lead to the optimal and practically viable Bragg breakwaters for real sea conditions.

References

Bailard, J. A., DeVries, J. W. and Kirby, J. T. (1992). Considerations in using Bragg reflection for storm erosion protection, *J. Waterway Port Coastal Ocean Eng.* **118**, 1, pp. 63–74.

Belzons, M., Rey, V. and Guazzelli, E. (1991). Subharmonic Bragg resonance for surface water waves, *Europhysics Letters* **16**, 2, pp. 189–194.

Benjamin, T. B., Boczar-Karakiewicz, B. and Pritchard, W. G. (1987). Reflection of water waves in a channel with corrugated bed, *J. Fluid Mech.* **185**: 249–274.

Berkhoff, J. C. W. (1972). Computation of combined refraction-diffraction, *Proc. 13th Int. Conf. Coastal Eng.*, ASCE, pp. 471–490.

Chamberlain, P. G. and Poter, D. (1995). The modified mild-slope equation, *J. Fluid Mech.* **291**: 393–407.

Cho, Y. S. and Lee, C. (2000). Resonant reflection of waves over sinusoidally varying topographies, *J. Coastal Research* **16**, 3, pp. 870–876.

Dalrymple, R. A. and Kirby, J. T. (1986). Water waves over ripples, *J. Waterway Port Coastal Ocean Eng.* **112**, 2, pp. 309–319.

Davies, A. G., Guazzelli, E. and Belzons, M. (1989). The propagation of long waves over an undulating bed, *Phys. Fluids* **1**: 1331–1340.

Davies, A. G. and Heathershaw, A. D. (1984). Surface wave propagation over sinusoidally varying topography, *J. Fluid Mech.* **144**: 419–443.

Guazzelli, E., Rey, V. and Belzons, M. (1992). Higher-order Bragg reflection of gravity surface waves by periodic beds, *J. Fluid Mech.* **245**: 301–317.

Hara, T. and Mei, C. C. (1987). Bragg scattering of waves by periodic bars: Theory and experiment, *J. Fluid Mech.* **178**: 59–76.

Hsu, T. W. and Wen, C. C. (2000). A study of using parabolic model to describe wave breaking and wide-angle wave incidence, *J. Chinese Institute of Eng.* **23**, 4, pp. 515–527.

Hsu, T. W. and Wen, C. C. (2001). A parabolic equation extended to account for rapidly varying topography, *Ocean Eng.* **28**: 1479–1498.

Kirby, J. T. and Dalrymple, R. A. (1983). Propagation of obliquely incident water waves over a trench, *J. Fluid Mech.* **133**: 47–63.

Kirby, J. T. (1986). A general wave equation for waves over rippled beds, *J. Fluid Mech.* **162**: 171–186.

Kirby, J. T. and Anton, J. P. (1990). Bragg reflection of waves by artificial bars, *Proc. 22th Int. Conf. Coastal Eng.*, ASCE, pp. 757–768.

Lee, C., Park, W. S., Cho, Y. S. and Suh, K. D. (1998). Hyperbolic mild-slope equations extended to account for rapidly varying topography, *Coastal Eng.* **34**: 243–257.

Li, B. (1994). An evolution equation for water waves, *Coastal Eng.* **23**: 227–242.

Liu, P. L.-F. (1983). Wave-current interactions on a slowly varying topography, *J. Geophysical Research* **88**: 4421–4426.

Maa, J. P.-Y., Hsu, T. W., Tsai C. H. and Juang W. J. (2000). Comparison of wave refraction and diffraction models, *J. Coastal Research* **16**, 4, pp. 1043–1082.

Mansard, E. P. D. and Funke, E. R. (1980). The measurement of incident and reflected spectra using a least squares method, *Proc. 17th Int. Conf. Coastal Eng.*, ASCE, pp. 154–172.

Mei, C. C. (1985). Resonant refection of surface water waves by periodic sandbars, *J. Fluid Mech.* **152**: 315–335.

Mei, C. C., Hara, T. and Naciri, M. (1988). Note on Bragg scattering of water waves by parallel bars on the seabed, *J. Fluid Mech.* **186**: 147–162.

Miles, J. W. (1981). Oblique surface-wave diffraction by a cylindrical obstacle, *Dynamics of Atmospheres and Oceans* **6**: 121–123.

O'Hare, T. J. and Davies, A. G. (1993). A comparison of two models for surface-wave propagation over rapidly topography, *Applied Ocean Research* **15**: 1–11.

Smith, R. and Sprinks, T. (1975). Scattering of surface waves by a conical island, *J. Fluid Mech.* **72**: 373–384.

Suh, K. D., Lee, C. and Park, W. S. (1997). Time-dependent equations for wave propagation on rapidly varying topography, *Coastal Eng.* **32**: 91–117.

Zhang, L., Kim, M. H., Zhang, J. and Edge, B. L. (1999). Hybrid model for Bragg scattering of water waves by steep multiply-sinusoidal bars, *J. Coastal Research* **15**, 2, pp. 486–495.